Research Article

SCIENCE PARK
PUBLISHER

Integrated Nano

Aminopropyl triethoxy silane capped ZnO quantum dots for highly selective dopamine

Zahraa Mohamed[1], Moataz Soliman[1], Ali Gad[1], Shaker M. Ebrahim[1], Yasmeen Elkony[1,2,*]

[1] Department of Materials Science, Institute of Graduate Studies and Research, Alexandria University, 163 Horrya Avenue, El-Shatby, P.O. Box 832, Alexandria, Egypt.

[2] Heavy Metal lab, Central labs of Ministry of Health, Alexandria, Egypt

Abstract

Quantum dots (QDs) can be used as labels with fluorescent nanoprobes and ZnO QDs have a band gap over 4 eV with a large 60 meV exciton binding energy. Capped ZnO presents high quantum efficiency and surface enhancement in biochemical analysis and ultrasensitive detection of biomaterials and proteins. This work reported the synthesis of ZnO QDs capped with different agents of 3-aminopropyl triethoxy silane (APTES), tetraethyl orthosilicate (TEOS) and dimethyl sulfoxide (DMSO) from a nonaqueous medium. ZnO QDs were characterized by different techniques of UV-vis absorption spectra, fluorescent emission spectra, X-ray diffraction (XRD), Fourier transform infrared (FTIR) spectroscopy, Zeta potential and high-resolution transmission electron microscopy (HRTEM). Photoluminescence (PL) emissions illustrated that APTES capped ZnO QDs have the highest PL intensity and applied as an optical sensor for dopamine (DA) determination in an aqueous solution and real serum samples. The visible luminescence of ZnO may result from either the recombination of a delocalized electron with a deeply trapped hole or the recombination of a delocalized hole with a deeply trapped electron. Zeta potential values showed that the surface potentials of - 4.23, -7.70, -14, -1.94 mV for uncapped ZnO, DMSO, APTES capped, and TEOS capped ZnO QDs, respectively. The fluorescence quenching observed in ZnO QDs primarily stemmed from electron transfer between the ZnO QDs and two variants of dopamine: reduced dopamine acting as electron donors and oxidized dopamine-quinone serving as electron acceptors. APTES capped ZnO QDs probe exhibited a linear dynamic range from 6.2 – 0. 195 nM of DA with correlation coefficient (R^2) of 0.99, limit of detection (LOD) of 0.2 nM and a sensitivity of 406.6 μM^{-1}.

1. Introduction

QDs as nanocrystals possess unique characteristics and exhibit fascinating phenomena such as size-dependent emission wavelength, narrow emission peak and a broad range of excitation possibilities [1-2].

QDs in which excitons are confined in three spatial dimensions and this is accomplished with that QDs consisting of several hundred to thousands of atoms and these QDs behave like artificial atoms.

Research Article

Louis E. Brus created QDs for the first time in the 1980s [3], and other fields were interested in these unique nano-structures because of their remarkable characteristics [4-6]. QDs can be optically stimulated: when a photon with a specific energy is absorbed, the electrons within the QDs absorb this energy and produce excitons. A hole is a quasi-particle and the exciton is a bound state of electrons. Exciton recombination is the process by which electrons and holes recombine, leading to the emission of photons with distinct energies after the relaxation of the excitonic excited state to its reduced energy state. The cycle of excited state relaxation, electron and hole recombination, optical excitation, and fluorescent emission is referred to as photoluminescence (PL). The quantity of photons discharged can be determined in relation to their energy, resulting in the PL spectrum.

QDs are susceptible to excitation across a broad spectrum of wavelengths due to their extensive and continuous absorption spectra. The light source can excite several forms of QDs, and their emissions can be separated. QD emission light spectra are more symmetrical and narrower than those of conventional organic dyes [7-9], resulting in a greater sensitivity than organic dyes.

The QDs are assumed to be attractive fluorophores for biological imaging due to this property (biological tagging) [4-6]. Zinc oxide quantum dots possess a wide band gap semiconductor, moreover, their unique optical and electronic properties involved it in various applications.

The nanoparticles ZnO are of special attention because the size, shape and defects of NPs are controlled by many ways to maintain their optical properties. For example, ultra-small ZnO NPs, also known as ZnO (QDs), have an expanding band gap because of quantum confinement, along with decreasing particle size. In addition, ZnO QDs are more stable and biocompatible with a large direct band gap. Although the bulk ZnO has a band gap of about 3.37 eV, ZnO QDs have over 4.0 eV due to the quantum confinement.

Dopamine as a hormone and neurotransmitter belongs to the catecholamine families and has been involved in regulating normal appetite behaviors including feeding, drinking, and pathological behaviors ranging from drug addiction to schizophrenia. Dopamine has a significant influence on the processing of information through its effects on excitement and vigilance, as well as on learning and memory. It is confirmed by its involvement in Parkinson's disease. These neurotransmitters are definitely the most appropriate for normal and abnormal behavior [10]. Normal range of dopamine in the human body is less than 30 pg/mL (195.8 pmol/L) [11].

QDs may be utilized as an alternative method for detecting dopamine in blood, in situations where fluorescent techniques are deemed cumbersome, expensive, and have a low detection limit. The biosensor that was developed to detect DA in human blood samples demonstrated a notable degree of selectivity towards DA, while avoiding the interference of biomolecules such as certain amino acids and chlorides [12].

This work aims to synthesize uncapped and capped ZnO QDs with different capping agents. These QDs are characterized by UV-vis absorption spectra, fluorescent emission spectra, X-ray diffraction (XRD), Fourier transform infrared (FTIR) spectroscopy, Zeta potential and high-resolution transmission electron microscopy (HRTEM). The evaluation of ZnO QDs probe for DA detection in the range from 6.2 to 0.195 nM based on the luminescence property is investigated and the quenching mechanism of ZnO QDs by DA interaction is proposed. The sensitivity, selectivity, correlation coefficient and limit of detection of this probe are determined. Moreover, the dopamine concentrations in real serum samples are measured.

2. Materials and Methods

2.1. Materials

Methanol absolute was obtained from El Nasr Pharm. Chem. Co. (Adwic) and zinc acetate dihydrate (purity 99%) was received from El Gomhoryia Pharm.Co. Dopamine hydrochloride was purchased from Sunny Pharm.Co. (3-Aminopropyl) triethoxysilane (APTES), tetraethyl orthosilicate (TEOS), dimethyl sulfoxide (DMSO), and KOH were purchased

Research Article

from Sigma-Aldrich. All the reagents were analytical grade and used without further purification.

## 2.2. Synthesis of uncapped ZnO and capped ZnO QDs

To produce nonaqueous ZnO QDs, a straightforward precipitation process was utilized. The synthesis of a 0.1 M zinc acetate solution involved the discrete dissolution of 0.55 g of zinc acetate in 25 mL of methanol and 2.8 g of KOH in 50 mL of methanol to produce a 1M (KOH) solution. The reaction was then conducted at room temperature while agitating continuously while adding KOH solution drop by drop to the zinc acetate solution. The solution was maintained at a final pH of approximately 12.5. The solution was subsequently homogenized through one hour of continuous magnetic agitation. Under UV excitation, the obtained solution emitted a brilliant bluish-green glow, which indicated the formation of ZnO particles.

At this stage, 2 mL (0.23 mmole) of APTES solution as a capping agent was added to the ZnO solution to control particle growth. The same steps were repeated with changing the capping agent in the second step by adding 2 mL of TEOS or DMSO. At the final the same steps were repeated but without adding any capping agent [13, 14]. An alternative and interesting

methodology to functionalize and stabilize the surface of ZnO nanocrystals is chemically based on organosilanes to inhibit decomposition in the aqueous media. Silane surface modification of ZnO nanoparticles has been used successfully to stabilize ZnO QDs in water. Trialkoxysilans are strongly related to hydroxylated surfaces and form covalent bonds with them [15].

APTES demonstrated complete solubility in both water and methanol solvents, with no sign of insolubility such as aggregation observed in the solvent system. Due to the inherent basic nature of its amino group, APTES undergoes autocatalysis in its hydrolysis and condensation processes, obviating the need for an additional catalyst in the modification procedure

Scheme 1 illustrates the proposed mechanism of the synthesized APTES functionalized ZnO QDs. APTES functionalized ZnO QDs were synthesized by the reaction between APTES and the hydroxyl groups on the ZnO surface in the presence of methanol [16]. Hydrolysis occurs in both APTES and ZnO and these form hydroxylated ZnO and silanol. The functionalization process of ZnO can occur through two paths; path (1) a condensation process is carried out where water molecules come out as a byproduct and path (2) can happen through the formation of hydrogen bonds between hydroxylated ZnO and APTES.
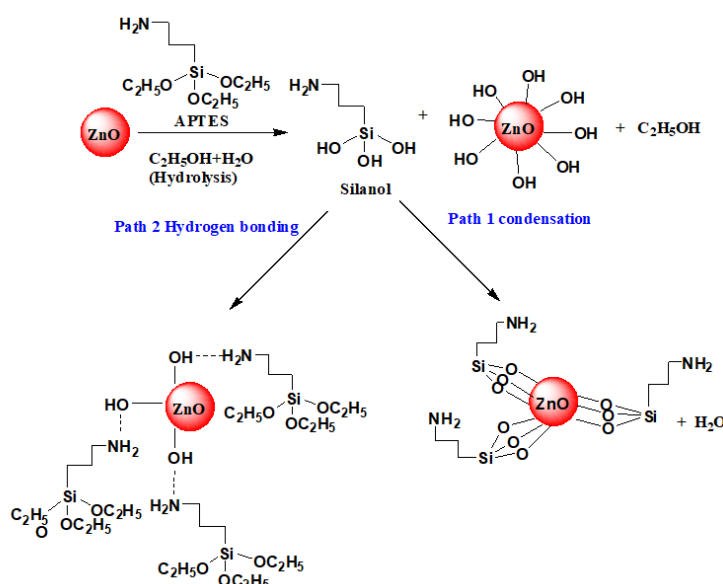
Scheme 1. Formation of APTES capped ZnO QDs.

Research Article

2.3. Detection of dopamine using luminescence spectra

The detection of different concentrations of dopamine (DA) was performed at room temperature and PH 12.5. The sensing experiments of (DA) were carried out by monitoring the PL behavior of the APTES capped ZnO QDs +DA solution. Briefly, series of concentrations of DA (0.0062-0.000195 µM) were prepared in a 25 ml volumetric flask and also the blank without adding the DA then 50 µL of APTES capped ZnO were added to these concentrations of previously prepared DA and the volumetric flask was completed to 25mLwith DI water. The PL spectra of the resulting solutions were recorded by the excitation wavelength 330 nm and the emission data were collected in the range from 400 to 600 nm.

2.4. Characterization techniques

The optical absorption spectra of solutions containing uncapped and encapsulated ZnO QDs were determined utilizing a Hitachi Evolution 600 thermos UV-vis spectrometer. An adjustment was made to the wavelength range from 200 nm to 800 nm at ambient temperature. The Perkin Elmer (LS 55) PL spectrometer was utilized for PL spectroscopy, with an excitation wavelength of 330 nm and a recording range of 200 to 900 nm.The molecular structures and functional groups of ZnO QDs samples obtained under different conditions were conveniently determined by FTIR spectroscopy (Spectrum BX 11 spectrometer FTIR PerkinElmer Spectrum Version 10.5.3). Moreover, the wavenumber ranged from 4000-400 cm^{-1} and the sample was mulled with dry KBr at room temperature. In addition, the crystal structure of the QDs was obtained based on the X-ray diffractometer (X-ray 7000 Shimadzu-Japan) at room temperature, using CuKa radiation at 30 kV and 30 mA and X-ray spectra range of the Braggs angle (2θ) was from 10° to 80° with a scan rate of 4 degree/min. The JEM-2100 HRTEM was utilized to scan the morphology images at an operating voltage of 20 to 200 kV. As a result, the specimens were diluted in ethanol before a single droplet was applied to a copper grid coated with 5 nanometer carbon film. The Zeta potential was also calculated utilizing a NanoZS/ZEN3600 Zetasizer. In order to conduct the zeta potential analysis, an attenuated sample was introduced into a platinum electrode-equipped universal folded capillary cell. The zeta potential values were calculated by averaging the observed electrophoretic mobility.

3. Results and Discussion

3.1. Optical and fluorescence properties of uncapped and capped ZnO QDs

The optical and PL spectra of the synthesized uncapped and capped ZnO QDs were measured at pH of 12.5 at room temperature using different capping agents (APTES, DMSO, TEOS) which are presented in Figure 1. The absorption spectrum of uncapped ZnO NPs and APTES, DMSO and TEOS capped ZnO QDs before and after adding 0.5 µM of DA. The absorption spectrum of uncapped ZnO shows a characteristic shoulder in the range around 315 nm, while the absorption spectra of APTES, DMSO and TEOS capped ZnO illustrate shoulders at 315, 335 and 285, respectively. The optical absorption of uncapped and capped ZnO samples after adding DA solution shows change in the intensity and location of the shoulder. For uncapped ZnO and DMSO capped ZnO QDs, the absorption peak of ZnO after adding DA indicates a red shift toward the longer wavelength for these shoulders [17].

On the other hand, APTES capped ZnO QDs displays a small blue shift with DA because of hydrogen bonding interaction [14]. While, TEOS capped ZnO QDs appear no change in the absorbance after adding DA. It's observed that the absorption peak of the prepared ZnO samples exhibits a decrease in intensity and broadening after the addition of dopamine. This effect occurs because the catechol groups of dopamine undergo oxidation during self-polymerization, resulting in the generation of a significant amount of melanin. Melanin, in turn, absorbs ultraviolet and visible light across a wide range, leading to the broadened absorption spectrum observed. Additionally, the high-intensity band in the absorbance spectrum of ZnO is attributed to the strong absorbance characteristic of ZnO nanoparticles [18]. Therefore, in the prepared capped and

Research Article

uncapped ZnO NPs and QDs samples, the absorbance declines after adding DA.

ZnO optical band gap can be estimated by applying the Tauc's equation which illustrates a relationship between the coefficient of absorbance and the incident photon energy of ZnO. The optical band gap is obtained by using the following equation (1) [20, 21]

$$\alpha h\upsilon = A(h\upsilon - E_g)^n \qquad (1)$$

In this context, A represents a constant, E_g indicates the optical band gap of ZnO, and the exponent n is a variable that varies with the nature of the transition. Directly permitted, indirectly permitted, and directly prohibited transitions have n values of 1/2, 2 and 3/2, respectively. n is denoted as 1/2 in ZnO [19, 20]. The calculation of the E_g of ZnO can be accomplished by extrapolating the linear portion of the absorption edge from the plot of $(\alpha\upsilon h)^2$ against $(h\upsilon)$, as illustrated in Figure 2. The calculated values of band gaps of ZnO prepared samples are illustrated in the following table1.

Table 1. The calculated band gaps of ZnO samples.

Sample	Free ZnO QDs / NPs (E_g) eV	0.5 µM DA /ZnO QDs, NPs solution (E_g) eV
Uncapped ZnO NPs	3.3	3
APTES capped ZnO QDs	3.6	3.1
DMSO capped ZnO QDs	3.46	3
TEOS capped ZnO NPs	2.5	2.6

The decrease in band gap energy values after adding DA solutions may be attributed to an increase in the electron mobility upon melanin incorporation in the ZnO nanostructure [18], The initiation of the band edge has been observed to shift towards the blue region of the spectrum in ZnO quantum dots (QDs) capped with APTES and DMSO, where the band gap value decreases with increasing electron mobility. These results indicate that the absorption characteristics of ZnO quantum dots (QDs) prepared with different capping agents are affected by their size. Furthermore, the band gap value is influenced by quantum

confinement effects. [13]. This indicates spatial confinement of the photogenerated charge carriers observed when the size of ZnO particles is smaller 5 to 6 nm [21]. The small band gap value of TEOS capped ZnO NPs reflects the large particle size of this prepared ZnO.

PL spectra of ZnO QDs with different capping agents under excitation of 330 nm are presented in Figure 3. Two emission bands are discernible: one is comparatively narrow and faint, peaking at approximately 370 nanometers, and is attributed to the radiative recombination of excitons. Trap emission is a broad and concentrated phenomenon that is centered in the visible spectrum between 400 and 600 nanometers. The green-yellow emission of ZnO quantum dots is generally more conspicuous in contrast to the blue emission.

The green-yellow emission is caused by electrons or holes that have become entangled in the oxygen vacancies on the ZnO surface; furthermore, it is challenging to ascertain the energetic location of the trapped carriers. Furthermore, the visible luminescence observed in ZnO may be attributed to either a delocalized electron recombination with a deeply trapped hole or a delocalized hole recombination with a deeply trapped electron. The origin of the blue emission is seldom analyzed, in contrast to the green-yellow emission of ZnO nanoparticles, which is commonly associated with this process. The only emission associated with the mechanism is the green-yellow one emitted by ZnO nanoparticles; the source of the blue emission is seldom investigated. Blue fluorescence can be defined as the result of an electron transitioning from a state near the conduction band to a superficially confined hole in a vacancy on the ZnO surface, which is slightly higher in energy than the ZnO valence band [22].

The peak intensity varied with various capping agents, as shown in Figure 3. APTES-capped ZnO QDs generate the maximum intensity, whereas TEOS-capped ZnO NPs produce the lowest intensity.

The intensity of PL emission diminishes as the size of the ZnO samples increases. The relationship between emission intensity and surface properties, as well as dimensions, is widely

Research Article

recognized. Nevertheless, the structure and optical properties are guaranteed to be influenced by the surface states of nanocrystals. A ZnO particle with a dimension of approximately 3 nm exhibits a molecular content of nearly 50%, indicating that the majority of emissions originate from defects present on the QD surface. In addition, as particle size increases, the rate of surface trapping decreases, as does the rate at which a hole trapped at the surface emission mechanisms that can be attributed to ZnO QDs. Due to the direct correlation between the band gap and the recombination of the photogenerated electron with a hole within the valence band, this emission is size dependent by virtue of quantum confinement. The origin of visible luminescence, which is also referred to as deep-level emission, is a more intricate matter. Various proposed mechanisms attempt to elucidate this phenomenon, including oxygen vacancies (VO)

tunnels towards the center, in addition to the rate at which an electron conduction band is trapped at the surface. Due to the high surface-to-volume ratio and particle growth in nanocrystals, defect centers are more concentrated at the surface. As a consequence, the process of surface trapping diminishes, leading to a reduction in the intensity of PL emission in ZnO QDs with larger particle sizes [13]. Figure 4 depicts the two potential and zinc vacancies (VZn). Two of the most frequently referenced mechanisms pertain to oxygen vacancies. The initial process involves the recombination of an electron that is superficially confined with a profound trap hole (Figure 4a). The second is that the photogenerated hole recombinates with an electron to occupy a solitary oxygen vacancy in the valence band (Figure 4b) [15].
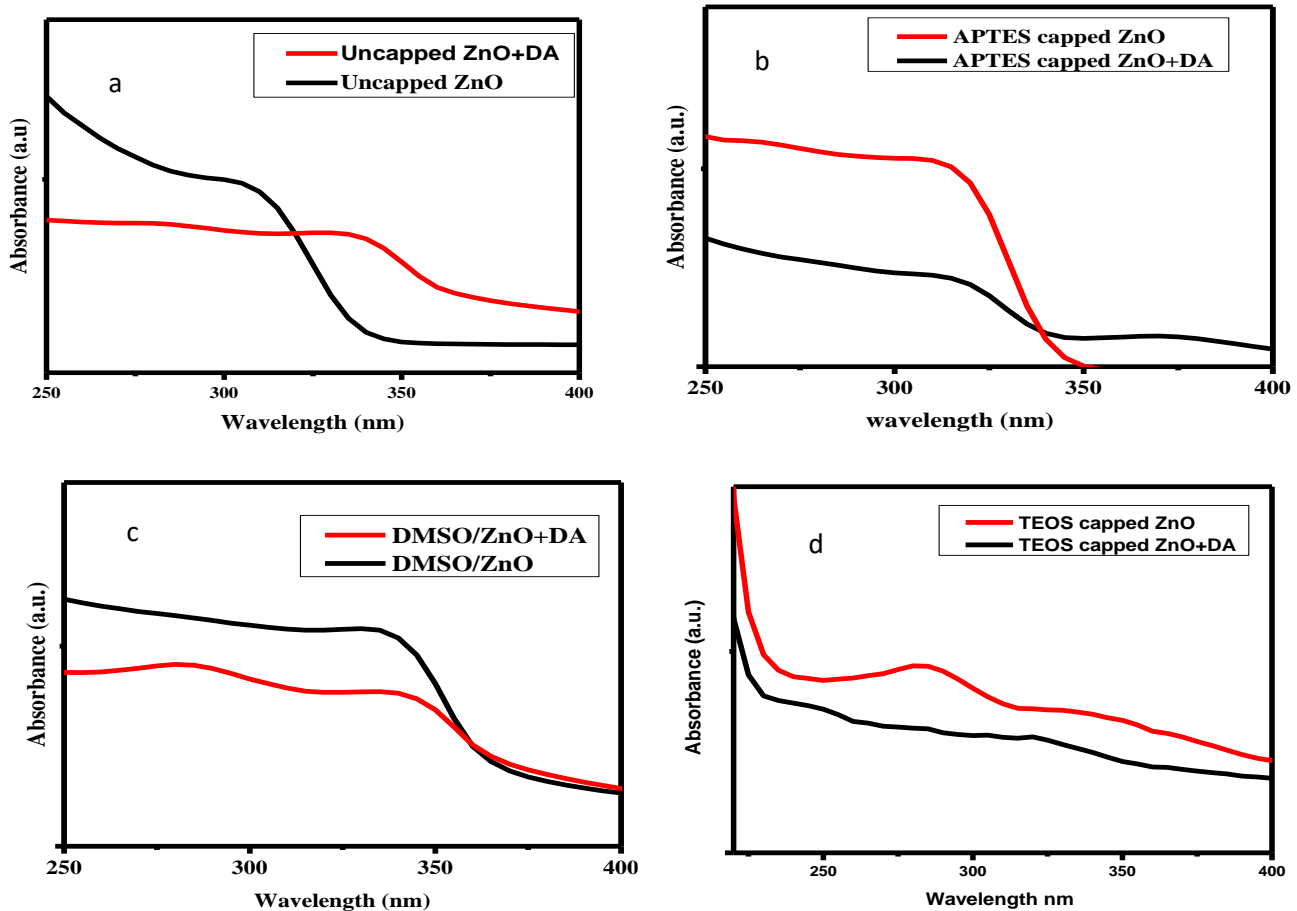

Figure 1. UV-Vis spectra of a) uncapped ZnO and uncapped ZnO/DA, b) APTES capped ZnO and APTES capped ZnO+DA, C) DMSO capped ZnO and DMSO capped ZnO+ DA d) TEOS capped ZnO and TEOS capped ZnO+DA.
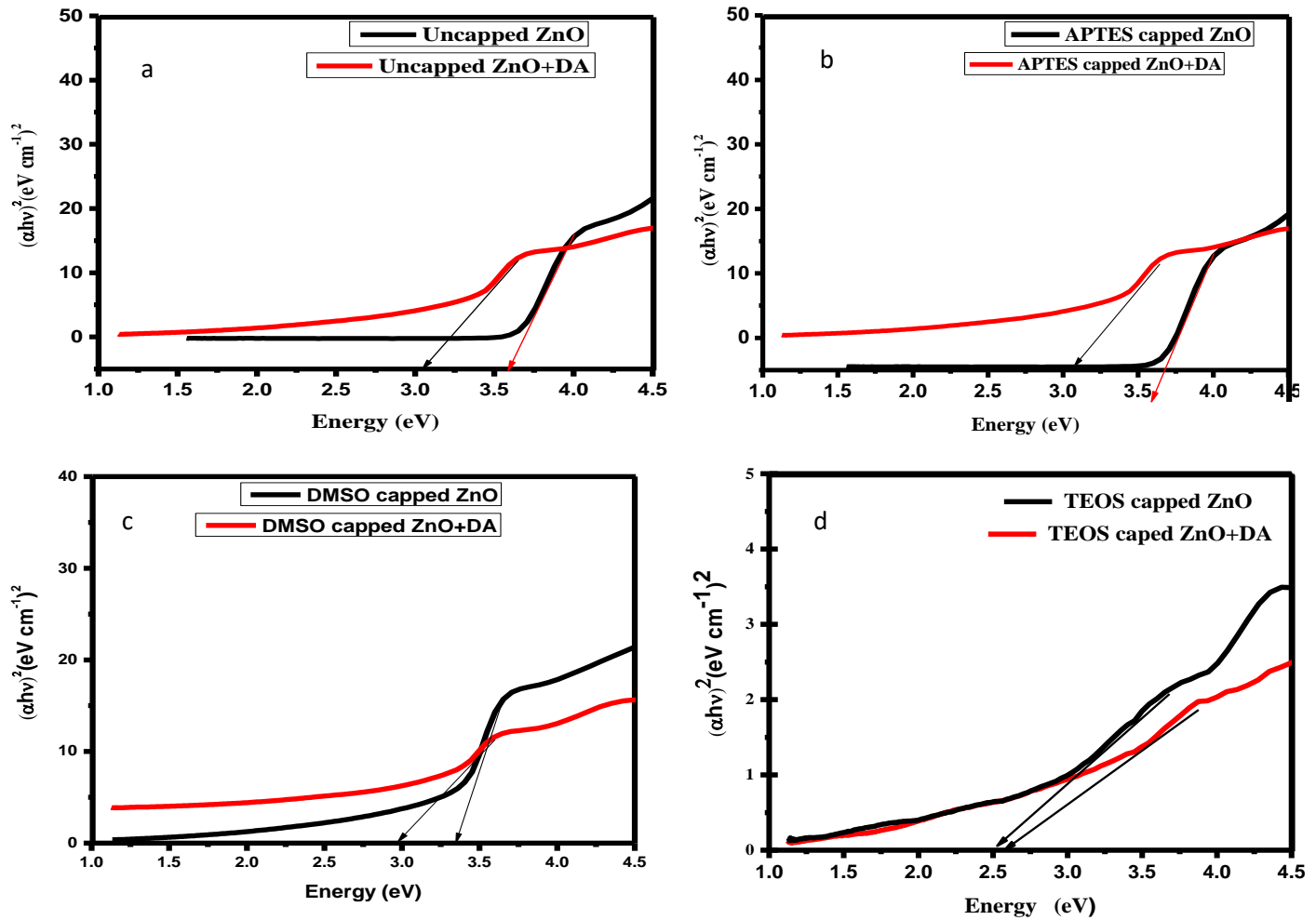
Research Article

Figure 2. Tauc's plots of a) uncapped ZnO and uncapped ZnO/DA, b) APTES capped ZnO and APTES capped ZnO+DA, C) DMSO capped ZnO and DMSO capped ZnO+ DA d) TEOS capped ZnO and TEOS capped ZnO+DA.
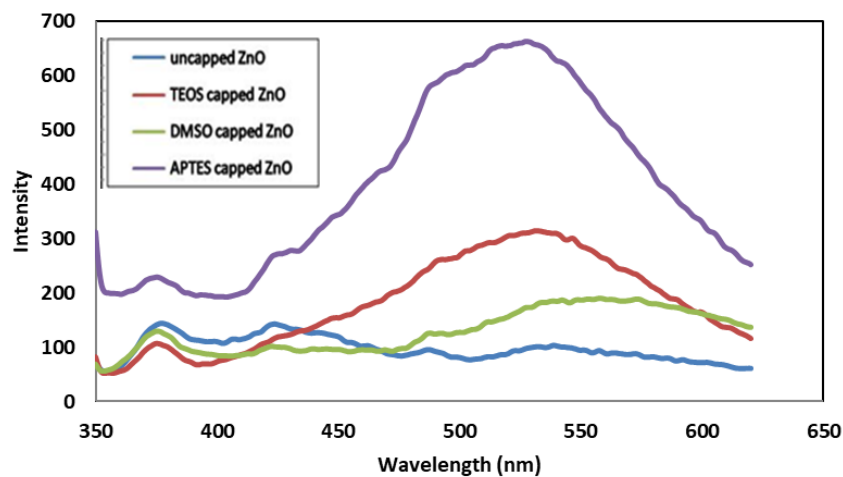

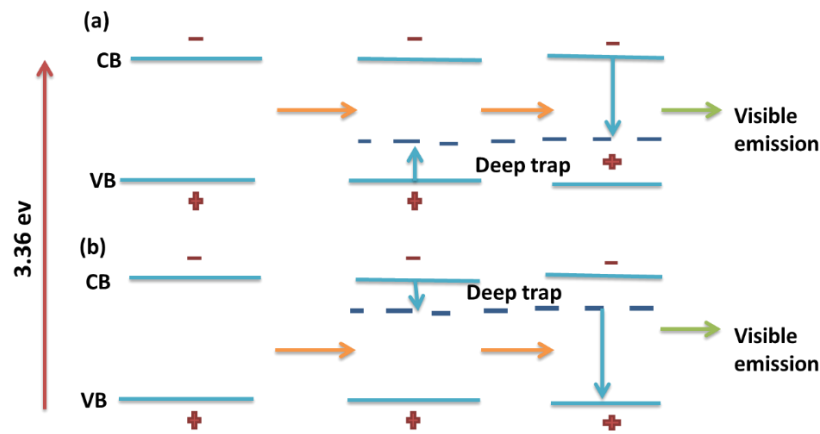**Figure 3.** PL spectra of ZnO with different capping agents.

Research Article

Figure 4. Defect emission of ZnO quantum dots.

3.2. Structural and morphological analysis of uncapped and capped ZnO QDs/NPs

Figure 5 illustrates the XRD structure patterns of uncapped and capped ZnO QDs/NPs synthesized at a reaction time of 120 minutes, 12.5 degrees Celsius, and 25 degrees Celsius. The principal peaks, which are situated at 32.17, 34.74, 36.55, 47.94, 56.7, 63.13, and 64.8, are, successively, associated with the (100), (002), (101), (102), (110), and (200) planes [23]. The patterns corresponded well to ZnO, which possesses a hexagonal wurtzite structure (JCPDS card No. 89-1397), and the pure phase generated extremely pointed and intense peaks [24], indicating a highly crystalline state. Additional diffraction peaks stem from impurity phases. The lack of variation in the XRD profiles of the capped ZnO QDs and NPs indicates that the QDs are in pure phase and that capping has not altered the hexagonal wurtzite structure of ZnO. [25].
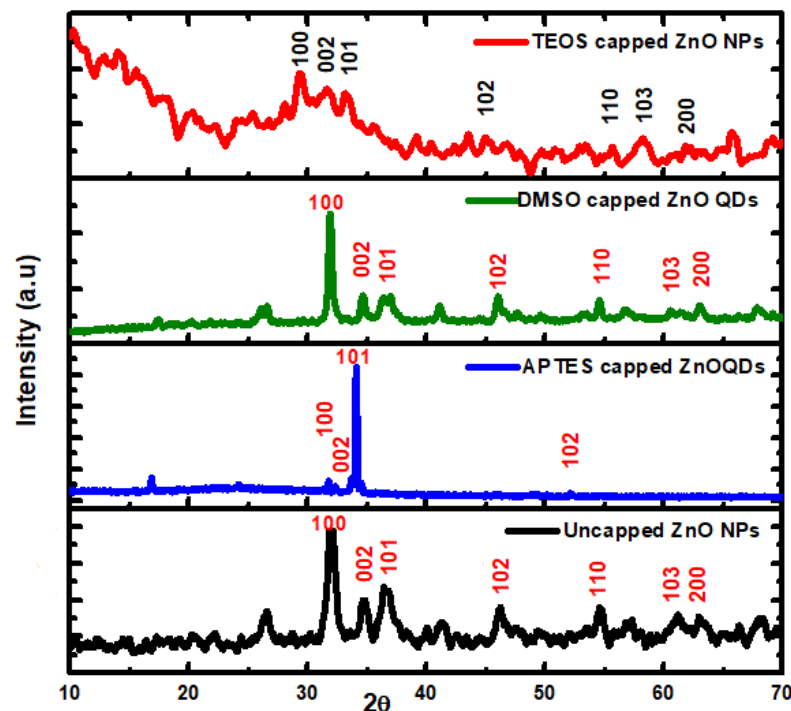

Figure 5. XRD patterns of uncapped and capped ZnO QDs/NPs.

Research Article

Interplanar distance (d) of the diffraction peaks is calculated using Bragg's equation (2), as shown in following Table 2.

$$n \lambda = 2 d \sin \theta \quad (2)$$

where θ is angle of incidence, λ is the wavelength of incident X-ray and n is integer number [26].

Table 2. Planes and their corresponding 2θ of the prepared ZnO samples.

d (hkl) \ sample	d(100)	d(002)	d(101)	d(102)	d(110)	d(103)	d(200)
Un capped ZnO	2.79	2.46	2.44	1.89	1.61	1.45	1.43
APTES capped ZnO	2.76	2.66	2.63	1.75			
DMSO capped ZnO	2.76	2.59	2.47	1.90	1.64	1.46	1.43
TEOS capped ZnO	2.9	2.79	2.58	1.92	1.53	1.44	1.40

It's noticed from XRD data there is no change in the wurtzite peaks after adding the capping agents which confirms that all the samples remain in hexagonal wurtzite structure as the lattice spacing which calculated corresponds to the lattice spacing of the wurtzite ZnO.

Broaden of diffraction peaks are influenced by crystallite size (D), so, the average crystallite size could be determined by using the Debye-Scherrer equation (3)

$$D = \frac{k\lambda}{\beta \cos \theta} \quad (3)$$

Where θ is the angle of incidence, λ is the wavelength of X-ray radiation, k is the shape factor (0.94), β is the full width at half maximum (FWHM) and D is the crystallite size [27]. The crystallite sizes of the samples were estimated with the (1 0 0) diffraction peak and calculated for different prepared ZnO samples as presented in Table 3.

Table 3. Crystallite size of different prepared ZnO samples.

Sample	D (crystallite size)
Uncapped ZnO	14.39 nm
DMSO capped ZnO	26.46 nm
APTES capped ZnO	47 nm
TEOS capped ZnO	134 nm

Typically, uncapped ZnO exhibits the tiniest crystallites, resulting in wide-ranging and inadequately defined peaks. The size of crystallites increases in capped samples relative to uncapped ZnO when specific concentrations of various capping agents are added; this results in more distinct and pointed diffraction peaks in the capped samples, which indicates the formation of a new crystalline phase [28]. The FTIR spectra of ZnO QDs/NPs, both untreated and sealed, are illustrated in Figure 6. The band at 3420 cm^{-1} is the result of the stretching vibration of the O-H bond of surface adsorbed hydroxyl groups and water in the case of uncapped ZnO NPs [24]. The peak observed at υ470 cm^{-1} is indicative of the stretching vibration of the Zn-O bond, while the peak at υ 2950 cm^{-1} is a result of the C-H bond stretching vibration [29]. The peaks observed within the range of υ 1400 to 1600 cm^{-1} correspond to carboxylate groups (-COO-), which are chemisorbed onto the surfaces of particles and provide a difficult-to-eradicate peak. [13]. The υ 1000-1100 cm^{-1} peaks are attributed to (C-OH) [25]. The samples' surfaces exhibit an adsorbed O=C=O (CO_2) impurity peak at approximately υ 2300 cm^{-1} in the FTIR spectra [30]. Upon FTIR analysis of ZnO QDs encapsulated with APTES, the stretching vibration of primary amine groups -NH_2 on the outer surface of the QDs was attributed to the peaks at υ 3400 cm^{-1} and 1650 cm^{-1} [31]. The peaks associated with the NH_2 group of APTES and the OH groups of the QDs overlapped. The vibration band associated with the stretching of (C-NH_2) groups is observed at υ 2920 cm^{-1} [16]. The bending stretching of (NH) groups is responsible

Research Article

for the peaks at υ 1480 cm^{-1} and 1386 cm^{-1}, whereas the stretching vibration of (C–N) groups is the cause of the peak at υ 990 cm^{-1} [16]. The wavelength of υ 1090 cm^{-1} is associated with the stretching vibration of Si–O. At υ 886 cm^{-1}, the Si–O–C peak is identified [19]. The peak near υ 670 cm^{-1} corresponds to the stretching vibration of zinc oxide. The broad absorption peak at υ 3409 cm^{-1} in the spectra of DMSO-capped ZnO QDs is attributed to the O-H bond. The O-S-O stretching bands, which are characteristic of DMSO, correspond to the peak near υ1030 cm^{-1}. The perturbation of the C-H bond is the cause of the band at υ 2895 cm^{-1}, which is more pronounced in the DAMSO-capped ZnO sample because of the methyl group of this capping compound [29]. A distinct absorption band at υ 486 cm^{-1} is present, which is indicative of the Zn-O bond. This finding suggests that the DMSO modification of the QDs surface was effectively carried out [29]. The presence of carboxylate groups adsorbed on the surfaces of particles is associated with peaks in the range of υ 1400 to 1600 cm^{-1} [13]. The peaks observed at υ 1000-1100 cm^{-1} are indicative of (C-OH) [25]. The presence of CO_2 impurities on the surface of the sample accounts for the peak at approximately υ 2300 cm^{-1} [30]. the TEOS-capped ZnO NPs' FTIR spectra. The identification of the absorption peaks at

approximately υ 1000 cm^{-1} and υ 710 cm^{-1} at an international location corresponds to the asymmetric and symmetric stretching of Si–O, respectively [32, 33]. In addition, the presence of a Zn–O–Si bond was suggested as the cause for the shoulder absorption bands at υ 870 cm^{-1} [28, 33]. The stretching vibration of the Si–OH bond is responsible for the presence of a small shoulder at υ 900 cm^{-1} [34]. A notable absorption peak is detected at υ 509 cm^{-1}, which is indicative of the stretching vibrations of Zn–O. The wavelength at which O-H stretching vibrations are absorbed is 3431 cm^{-1} [13]. The carboxylate group residuals that have adsorbed onto the surfaces of particles are responsible for the peaks at υ 1400-1600 cm^{-1} [13]. The band associated with the (CH) group, which is situated at υ 289 cm^{-1}, is either undetectable or too small to be detected in TEOS-capped ZnO. This is because the silica capping process completely hydrolyzed all CHX groups that were initially present in the TEOS structure, leaving behind a negligible quantity of ethoxy groups that could not be detected [34]. According to these findings, TEOS hydrolysis and condensation continued, and it is likely that hydrolyzed TEOS forms a silica encapsulating layer by interacting with the hydroxyl groups on the ZnO surface [33, 35].
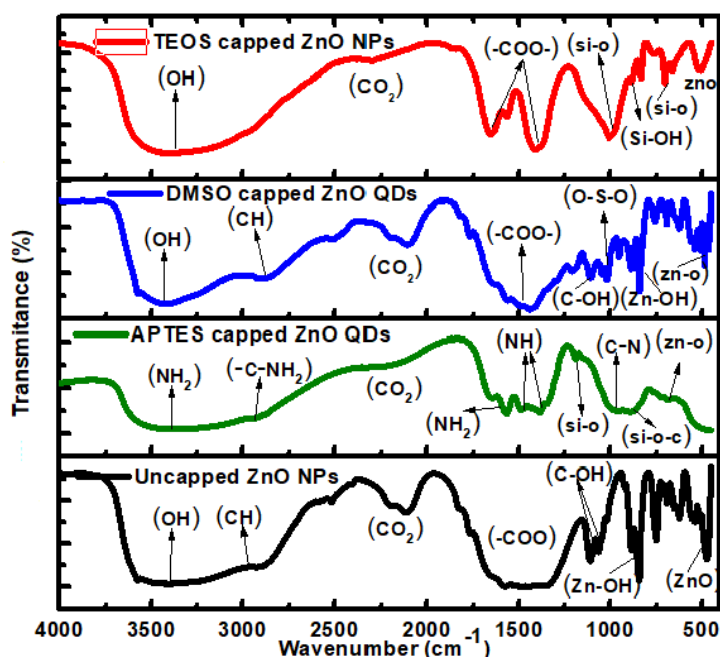

Figure 6. FTIR spectra of uncapped and capped ZnO QDs/NPs.

Research Article

3.3. Morphological properties of uncapped and capped ZnO QDs/NPs

The surface morphologies and crystallinities of uncapped and capped ZnO QDs/NPs are investigated in Figure 7. As shown in the HRTEM images in Figure 7 (a,b), the uncapped ZnO NPs have a uniform monodispersed hexagonal shape with an average particle size of approximately 170-270 nm. Some areas of the sample of the NPs scatter or absorb electrons and therefore appear darker regions. Other areas transmit electrons and appear brighter regions. [36]

Coagulation, agglomerations, and rod-shaped microcrystals measuring 800 nm in length and 430 nm in diameter are observed. The majority of ZnO rods have two distinct topographic characteristics: one is thicker and the other is thinner. The extremities of both the broader and thinner sections of the rod are plain-shaped [37]. APTES QDs were terminated with ZnO. ZnO QDs are monodisperse and homogeneous, with an approximate average particle size of 5-10 nm. The absence of the silane coating in the HRTEM image indicates that the coating on the surface is exceedingly thin. The HRTEM image inset illustrates the lattice space, which is 0.3 nm in size and corresponds to the interplanar distances of the wurtzite ZnO (100) planes [14]. When APTES is employed as a capping agent, there is a conspicuous reduction in the particle size of ZnO NPs in comparison to those that are not capped (Figure 7 (c,d)). The uniform elongated spherical shape of the DMSO-capped ZnO QDs may be attributed to the modification of the ZnO QDs' surface with DMSO, resulting in an average particle size of 7-10 nm (Figure (e,f)). In comparison to unsealed ZnO nanoparticles, the application of DMSO as a capping agent resulted in a reduction in particle size and an alteration of the surface morphology of ZnO. There are rod-shaped microcrystals and hexagonal-shaped ZnO NPs crowned with TEOS, measuring approximately 250 nm in length. ZnO filaments possess two distinct topographic characteristics: one is thicker and the other is slimmer. As illustrated in Figure 7 (g,h), both the thicker and thinner sections of the rod have plain-shaped extremities [37, 38]

and evident particle aggregation. The utilization of TEOS as a capping agent leads to elevated turbidity, agglomeration, and an enlargement of ZnO NPs, suggesting that TEOS is an ineffective capping agent.

Zeta potential values show that the surface potentials of ZnO NPs/QDs samples have small negatively charges of approximately - 4.23, -7.70, -14, -1.94 mV for uncapped, DMSO capped, APTES capped, TEOS capped ZnO, respectively. The zeta potential is applied to study the nanocrystals stability and from the value of APTES capped ZnO QDs, it can be concluded that it is more stable than others ZnO QDs [39].

3.4. Sensitivity and limit of detection of APTES capped ZnO QDs dopamine sensor

PL intensity of APTES capped ZnO QDs have a great effect with different concentrations of DA at pH of 10.5 as depicted in Figure 8. The APTES capped ZnO QDs fluorescence spectra display an emission band at 540 nm under excitation of 330 nm. ZnO QDs have been prepared in non-aqueous phase using APTES as a capping agent, leading in the connection of the silane groups to the surface of ZnO QDs, whereas the functional amino groups are free, that could easily be combined with biomolecules, such as proteins and peptides. The emission of ZnO QDs has been decreased successively with increasing concentration of DA. By adding of DA to the solution of QDs results in a quenching of QDs fluorescence without shift of fluorescence emission peak. The quenching effect is a result of the electron transfers that taking place between QDs and DA [40].

With an R^2 of 0.99, Figure 8 illustrates an inset of the linear relationship between the intensity of emission peaks of APTES-capped ZnO QDs and various concentrations of DA ranging from 0.006 to 0.00156M. The sensitivity is 406.6 M^{-1} and the LOD is determined to be 0.0002 µM. Presumably, the effective electron transfer (ET) that occurs between QDs and DA is what causes the quenching effect depicted in Figure 8. The observed results can be attributed to an electron transfer occurring between QDs and oxidized dopamine-quinone (electron acceptors) and

Research Article

reduced dopamine (electron donors), due to the dopamine redox activity. In this study, however, the experiments were conducted in an alkaline environment (pH 10.5). DA in an alkaline solution is susceptible to oxidation by ambient O_2 quinones, which for ZnO QDs function as electron acceptors [41-44]. The quenching mechanism of the fluorescence probe is illustrated in

Scheme (2). The introduction of a DA solution sample onto APTES-capped ZnO QDs induces strong noncovalent interactions, including electrostatic and hydrogen bonding. As a consequence, an electron transfer occurs from the photoexcited QDs to the oxidized dopamine-quinone, which ultimately leads to the quenching of fluorescence by the ZnO QDs [14].
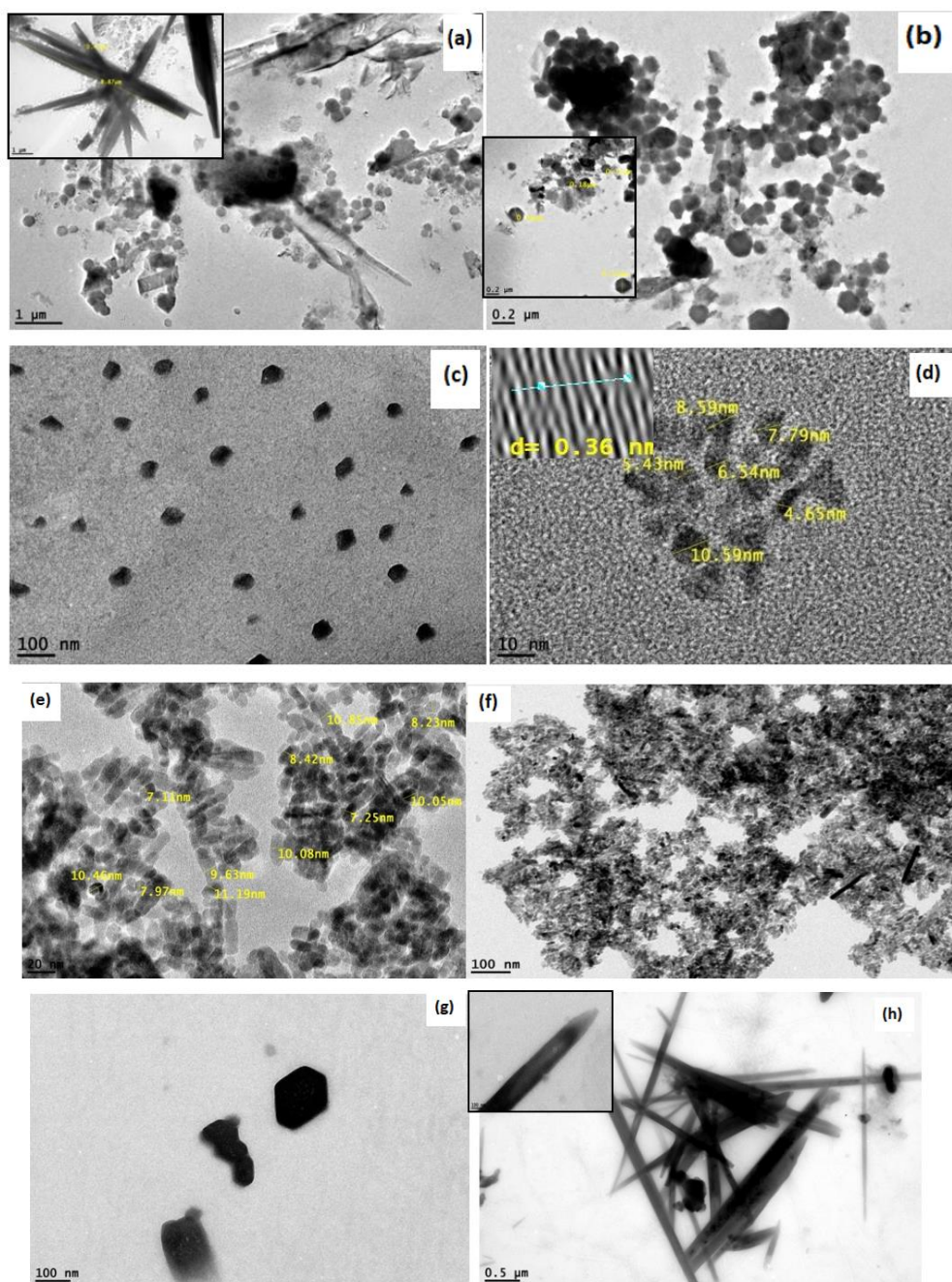

Figure 7. HRTEM images of uncapped ZnO NPs at different magnifications with inset of (micro-rods and hexagonal NPs) (a,b), APTES capped ZnO QDs at different magnifications with inset of lattice space (c,d), DMSO capped ZnO QDs (e,f) and TEOS capped ZnO NPs (g,h) with inset of micro-rods.
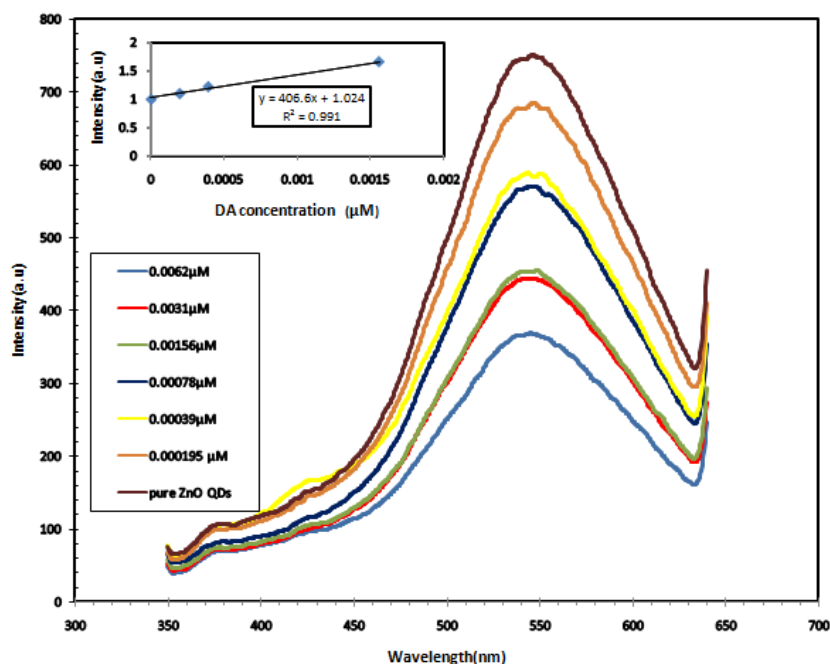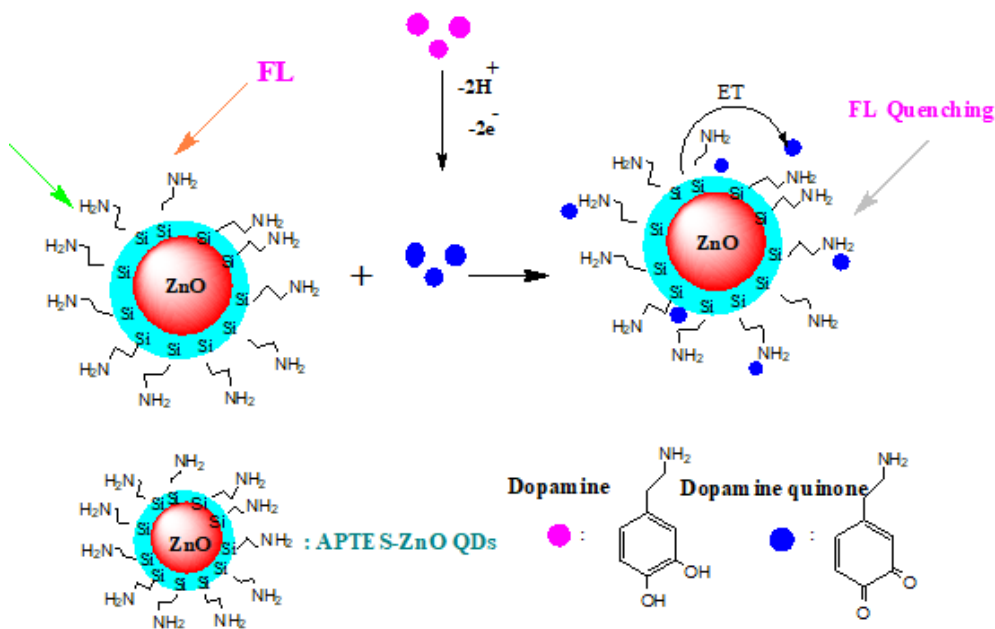
Figure 8. PL intensity of APTES capped ZnO QDs vs. concentrations of DA.

Scheme 2. Schematic illustration of the developed APTES capped ZnO QDs-based fluorescent probe for DA detection.

3.5. Interference and selectivity of dopamine

In the context of actual sample detection, in addition to the criticality of high sensitivity, high specificity is also ideal. Impediment from common molecules found in human blood serum was examined in order to validate the efficacy of APTES-capped ZnO QDs as a DA probe on actual samples. The effect of various biomolecules, such as urea, ascorbic acid (AA), glucose, and cholesterol, with concentrations of 0.001μL also examined, as illustrated in Figure 9. alongside DA. Where the

Research Article

quenching efficiency (QE) was calculated using this Equation (4) [45]

$$QE = F° − F/F° \qquad (4)$$

Where F° and F represent the PL intensities of APTES capped ZnO QDs in the absence and presence of guest molecules.

 APTES-capped ZnO QDs are marginally quenched by glucose, AA, cholesterol, and urea, resulting in 11%, 14%, 17%, and 20%

reductions in PL intensity, respectively. The most potent PL quenching is 32% brought about by DA. The emission of excited electrons from the QDs is transferred to the adsorbed DA on the surface of the APTES-capped ZnO QDs, which causes a quenching effect in the PL spectra of the QDs [14].
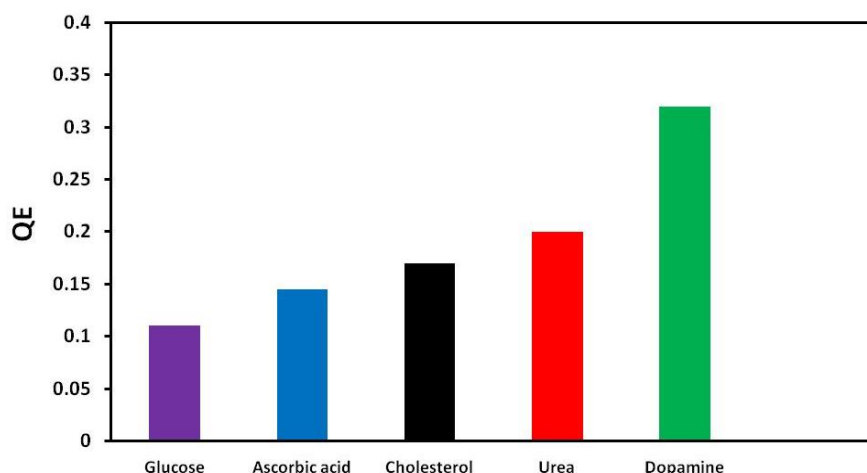

Figure 9. Selectivity bar chart of QE for different biomolecules.

4. Conclusion

The uncapped and capped ZnO QDs were successfully synthesized by a nonaqueous precipitation method at room temperature with different capping agents at pH 12.5. The PL studies occurred at excitation 330 nm, illustrated that the uncapped and capped ZnO QDs have a characteristic peak at around 540 nm. The visible luminescence mechanism of ZnO could be based on either a recombination of a delocalized electron with a deeply trapped hole or a recombination of a delocalized hole with a deeply trapped electron. The PL emission of APTES capped ZnO showed an increase in intensity more than others types of ZnO. The detection of DA was determined using all prepared ZnO NPs/QDs in the range from 0.0015 to 0.000195µM. It was observed that APTES capped ZnO QDs probe for DA has R^2 of 0.998 and LOD of 0.0002 µM. APTES

capped ZnO QDs showed a good sensitivity and selectivity for DA among different biological molecules.

Author Information

Corresponding Author: Yasmeen Elkony[*]

E-mail: igsr.yasmeen.elkony@alexu.edu.eg

References

[1] Ashoori, R. C. (1996). Electrons in artificial atoms. Nature, 379, 413. https://doi.org/10.1038/379413a0

[2] Alivisatos, A. P. (1996). Semiconductor clusters, nanocrystals, and quantum dots. Science, 271, 933. https://doi.org/10.1126/science.271.5251.933

[3] Brus, L. E. (1984). Electron–electron and electron-hole interactions in small semiconductor crystallites: The size dependence of the lowest excited electronic state. The

Research Article

Journal of Chemical physics, 80, 4403. https://doi.org/10.1063/1.447218

[4] Gao, X., Cui, Y., Levenson, R. M., Chung, L. W., and Nie, S. (2004). In vivo cancer targeting and imaging with semiconductor quantum dots. Nature Biotechnology, 22, 969. https://doi.org/10.1038/nbt994

[5] Michalet, X., Pinaud, F. F., Bentolila, L. A., Tsay, J. M., Doose, S. J. J. L., Li, J. J., Sundaresan, G., Wu, A M., Gambhir, S. S., and Weiss, S. (2005). Quantum dots for live cells, in vivo imaging, and diagnostics. Science, 307, 538. https://doi.org/10.1126/science.1104274

[6] Ntziachristos, V., Tung, C. H., Bremer, C., and Weissleder, R. (2002). Fluorescence molecular tomography resolves protease activity in vivo. Naturemedicine, 8, 757. https://doi.org/10.1038/nm729

[7] Bruchez, M., Moronne, M., Gin, P., Weiss, S., and Alivisatos, A. P. (1998). Semiconductor nanocrystals as fluorescent biological labels. Science, 281, 2013. https://doi.org/10.1126/science.281.5385.2013

[8] Chan, W. C., and Nie, S. (1998). Quantum dot bioconjugates for ultrasensitive nonisotopic detection. Science, 281, 2016. https://doi.org/10.1126/science.281.5385.2013

[9] Larson, D. R., Zipfel, W. R., Williams, R. M., Clark, S. W., Bruchez, M. P., Wise, F. W., and Webb, W. W. (2003). Water-soluble quantum dots for multiphoton fluorescence imaging in vivo. Science, 300, 1434. https://doi.org/10.1126/science.1083780

[10] Wenzel, A. (2017). The sage encyclopedia of abnormal and clinical psychology. SAGE Publications. https://doi.org/10.4135/9781483365817

[11] Young, W. F. (2007). Adrenal medulla, catecholamines, and pheochromocytoma. Cecil Medicine, 2, 1721. https://doi.org/10.1016/B978-1-4377-1604-7.00235-9

[12] Pourghobadi, Z., Mirahmadpour, P., and Zare, H. (2018). Fluorescent biosensor for the selective determination of dopamine by TGA-capped CdTe quantum dots in human plasma samples. Optical Materials, 84, 757. https://doi.org/10.1016/j.optmat.2018.08.003

[13] Patra, M. K., Manoth, M., Singh, V. K., Gowd, G. S., Choudhry, V. S., Vadera, S. R., and Kumar, N. (2009). Synthesis of stable dispersion of ZnO quantum dots in aqueous medium showing visible emission from bluish green to yellow. Journal of Luminescence, 129, 320. https://doi.org/10.1016/j.jlumin.2008.10.014

[14] Zhao, D., Song, H., Hao, L., Liu, X., Zhang, L., and Lv, Y. (2013). Luminescent ZnO quantum dots for sensitive and selective detection of dopamine. Talanta, 107, 133. https://doi.org/10.1016/j.talanta.2013.01.006

[15] Rahman, M. (2011). Nanomaterials. InTech Publisher, 27. https://doi.org/10.5772/1371

[16] Rabin, N. N., Morshed, J., Akhter, H., Islam, M. S., Hossain, M. A., Elias, M., Alam, Md. M., Karim, M. R., Hasnat, M. A., Uddin, Md. N., and Siddiquey, I. A. (2016). Surface modification of the ZnO nanoparticles with γ-aminopropyltriethoxysilane and study of their photocatalytic activity, optical properties and antibacterial activities. International Journal of Chemical Reactor Engineering, 14, 785. https://doi.org/10.1515/ijcre-2015-0141.

[17] Vairale, P., Sharma, V., Bade, B., Waghmare, A., Shinde, P., Punde, A., Doiphode, V., Aher, R., Pandharkar, S., Nair, Sh., and Jadkar, V. (2020). Melanin sensitized nanostructured ZnO photoanodes for efficient photoelectrochemical splitting of water: Synthesis and characterization. Engineered Science, 11, 76. http://dx.doi.org/10.30919/es8d0023.

[18] Ran, J., He, M., Li, W., Cheng, D., and Wang, X. (2018). Growing ZnO nanoparticles on

polydopamine-templated cotton fabrics for durable antimicrobial activity and UV protection. Polymers, 10, 495. https://doi.org/10.3390/polym10050495.

[19] Vishwakarma, J., Sabu, B., Bhotkar, K., Metha, S., and Muthurajan, H. (2016). Surface and band gap modification of ZnO nanoparticles to fine tune the optical properties. International Journal of Chemical and Physical Sciences, 5, 28.

[20] Musa, I., and Qamhieh, N. (2019). Study of optical energy gap and quantum confinement effects in zinc oxide nanoparticles and nanorods. Digest Journal of Nanomaterials and Biostructures, 14, 119.

[21] Panasiuk, Y. V., Raevskaya, O. E., Stroyuk, O. L., Kuchmiy, S. Y., Dzhagan, V. M., Hietschold, M., and Zahn, D. R. T. (2014). Colloidal ZnO nanocrystals in dimethylsulfoxide: A new synthesis, optical, photo-and electroluminescent properties. Nanotechnology, 25, 075601. https://doi.org/10.1088/0957-4484/25/7/075601.

[22] Neaime, C., Amela-Cortes, M., Grasset, F., Zakhour, M., and Molard, Y. (2016). Preparation of colloidal solution of silica encapsulating cyanobiphenyl unit-capped ZnO QD emitting in the blue region. Dalton Transactions, 45, 886. https://doi.org/10.1039/c5dt03851k.

[23] Wahab, R., Kim, Y. S., Lee, D. S., Seo, J. M., and Shin, H. S. (2010). Controlled synthesis of zinc oxide nanoneedles and their transformation to microflowers. Science of Advanced Materials, 2, 35. https://doi.org/10.1166/sam.2010.1064.

[24] Alshamsi, H. A. H., and Hussein, B. S. (2018). Hydrothermal preparation of silver doping zinc oxide nanoparticles: Study the characterization and photocatalytic activity. Oriental Journal of Chemistry, 34, 1898. https://doi.org/10.13005/OJC%2F3404025.

[25] Fu, Y. S., Du, X. W., Kulinich, S. A., Qiu, J. S., Qin, W. J., Li, R., Sun, J., and Liu, J. (2007). Stable aqueous dispersion of ZnO quantum dots with strong blue emission via simple solution route. Journal of the American Chemical Society, 129, 16029. https://doi.org/10.1021/ja075604i

[26] Meyers, H., and Myers, H. (1997). Introductory solid state physics. CRC press https://doi.org/10.1201/9780429320286.

[27] Kumar, C. G., Pombala, S., Poornachandra, Y., and Agarwal, S. V. (2016). Synthesis, characterization, and applications of nanobiomaterials for antimicrobial therapy. Nanobiomaterials in Antimicrobial Therapy, 103-152. https://doi.org/10.1016/B978-0-323-42864-4.00004-X.

[28] Rissi, N. C., Hammer, P., and Chiavacci, L. A. (2017). Surface modification of ZnO quantum dots by organosilanes and oleic acid with enhanced luminescence for potential biological application. Materials Research Express, 4, 015027. https://doi.org/10.1088/2053-1591/aa58fc.

[29] Esparza-González, S. C., Sánchez-Valdés, S., Ramírez-Barrón, S. N., Loera-Arias, M. J., Bernal, J., Meléndez-Ortiz, H. I., and Betancourt-Galindo, R. (2016). Effects of different surface modifying agents on the cytotoxic and antimicrobial properties of ZnO nanoparticles. Toxicology in Vitro, 37, 134. https://doi.org/10.1016/j.tiv.2016.09.020.

[30] Largani, S. H., and Pasha, M. A. (2017). The effect of concentration ratio and type of functional group on synthesis of CNT–ZnO hybrid nanomaterial by an in situ sol–gel process. International Nano Letters, 7, 25. https://doi.org/10.1007/s40089-016-0197-4.

[31] Moghaddam, E., Youzbashi, A. A., Kazemzadeh, A., and Eshraghi, M. J. (2015). Photoluminescence investigation of ZnO quantum dots surface modified with silane coupling agent as a capping agent. Journal of Luminescence, 168, 158. https://doi.org/10.1016/j.jlumin.2015.08.008

Research Article

[32] Bellamy, L. J. (1976). The infrared spectra of complex molecules, Vol. 1, Chapman and Hall Ltd., London, 80(1), 99. https://doi.org/10.1002/bbpc.19760800121

[33] Furusawa, T., Kadota, Y., Matsuzuka, A., Kurayama, F., Bahadur, N. M., Sato, M., and Suzuki, N. (2014). Surface modification of silica coated ZnO nanoparticles with 3-aminopropyltriethoxysilane by microwave-assisted method and its effect on the properties of coated samples. Journal of Chemical Engineering of Japan, 47(12), 900. https://doi.org/10.1252/jcej.14we164

[34] Hung, C. H., and Whang, W. T. (2005). Effect of surface stabilization of nanoparticles on luminescent characteristics in ZnO/poly (hydroxyethyl methacrylate) nanohybrid films. Journal of Materials Chemistry, 15(2), 267. https://doi.org/10.1039/b405497k

[35] Wu, Y. L., Tok, A. I. Y., Boey, F. Y. C., Zeng, X. T., and Zhang, X. H. (2007). Surface modification of ZnO nanocrystals. Applied Surface Science, 253(12), 5473. https://doi.org/10.1016/j.apsusc.2006.12.091

[36] Babayevska, N., Przysiecka, Ł., Iatsunskyi, I., Nowaczyk, G., Jarek, M., Janiszewska, E., and Jurga, S. (2022). ZnO size and shape effect on antibacterial activity and cytotoxicity profile. Scientific Reports, 12(1), 8148. https://doi.org/10.1038/s41598-022-12134-3

[37] Song, C., Sun, Y., Xu, Y., and Wang, D. (2011). Synthesis and optical property of ZnO nano-/micro-rods. Frontiers of Optoelectronics in China, 4(2), 156. https://doi.org/10.1007/s12200-011-0161-

[38] Khairnar, N., Kwon, H., Park, S., Lee, H., and Park, J. (2023). Tailoring the size and shape of ZnO nanoparticles for enhanced performance of OLED device. Nanomaterials, 13(21), 2816. https://doi.org/10.3390/nano13212816

[39] Saber, G., El-Dissouky, A., Badie, G., Ebrahim, S., and Shokry, A. (2023). Capped ZnO quantum dots with a tunable photoluminescence for acetone detection. RSC advances, 13(24), 16453. https://doi.org/10.1039/D3RA00491K

[40] Singh, P., Singh, R. K., and Kumar, R. (2021). Journey of ZnO quantum dots from undoped to rare-earth and transition metal-doped and their applications. RSC advances, 11(4), 2512. https://doi.org/10.1039/D0RA08670C

[41] Medintz, I. L., Stewart, M. H., Trammell, S. A., Susumu, K., Delehanty, J. B., Mei, B. C., and Mattoussi, H. (2010). Quantum-dot/dopamine bioconjugates function as redox coupled assemblies for in vitro and intracellular pH sensing. Nature Materials, 9(8), 676. https://doi.org/10.1039/D0RA08670C

[42] Banerjee, S., Kar, S., Perez, J. M., and Santra, S. (2009). Quantum dot-based off/on probe for detection of glutathione. The Journal of Physical Chemistry C, 113(22), 9659. https://doi.org/10.1021/jp9019574

[43] Gill, R., Freeman, R., Xu, J. P., Willner, I., Winograd, S., Shweky, I., and Banin, U. (2006). Probing biocatalytic transformations with CdSe− ZnS QDs. Journal of the American Chemical Society, 128(48), 15376. https://doi.org/10.1021/ja066636t

[44] Ji, X., Palui, G., Avellini, T., Na, H. B., Yi, C., Knappenberger Jr, K. L., and Mattoussi, H. (2012). On the pH-dependent quenching of quantum dot photoluminescence by redox active dopamine. Journal of the American Chemical Society, 134(13), 6006. https://doi.org/10.1021/ja300724x

[45] Ebrahim, S., Shokry, A., Khalil, M. M. A., Ibrahim, H., & Soliman, M. (2020). Polyaniline/Ag nanoparticles/graphene oxide nanocomposite fluorescent sensor for recognition of chromium (VI) ions. Scientific Reports, 10(1), 13617. https://doi.org/10.1038/s41598-020-70678-8